Published in J. Sol. Energy Eng., Vol. 134, Issue 3, August 2012

Experimental Study to Characterize the Performance of Combined Photovoltaic/Thermal Air Collectors

Véronique Delisle[1], Michaël Kummert[2]
[1] Natural Resources Canada, CanmetENERGY, 1615 Lionel-Boulet, Varennes, Québec, J3X 1S6, Canada, tel +1-450-652-7948, fax +1-450-652-5177, veronique.delisle@nrcan.gc.ca
[2] École Polytechnique de Montréal, PO Box 6079 STN Centre-ville, Montréal, Québec, H3C 3A7, Canada, tel +1-514-340-4711 x4507, fax + 1-514-340-5917, michael.kummert@polymtl.ca

Abstract

Background: Combined photovoltaic/thermal (PV/T) collectors show great potential for reaching the objective of net-zero energy consumption in buildings, but the number of products on the market is still very limited. One of the reasons for the slow market uptake of PV/T collectors is the absence of standardized methods to characterize their performance. Performance characterization is a challenge for PV/T collectors because of the interaction between the thermal and electrical yield. This study addresses this particular issue for PV/T air collectors used in either closed-loop or open-loop configurations. In particular, it presents the potential of the equivalent cell temperature method to determine the temperature of the PV cells in a PV/T air collector and validates models to predict the thermal performance and cell temperature for this particular type of solar collector. **Method of Approach**: Indoor and outdoor experimental tests were performed on two c-Si unglazed PV/T modules. The indoor part of this procedure provided the thermal diode voltage factor and the open-circuit voltage temperature coefficient, two parameters that are essential in the calculation of the equivalent cell temperature. The outdoor procedure consisted of acquiring simultaneous electrical and thermal measurements at various inlet temperatures and flowrates. **Results**: For the collector used in a closed-loop configuration, thermal efficiency models using the fluid inlet, outlet or average temperature in the calculation of the reduced temperature provided similar results. For an open-loop configuration, a thermal efficiency model as a function of the fluid outlet flowrate was found to be more appropriate. Using selection of variable methods, it was found that a multiple linear regression model using the fluid inlet temperature, the irradiance and the fluid outlet temperature as predictive variables could be used to estimate both the PV module back surface average temperature and the equivalent cell temperature. When using the PV temperature predicted by these models in the electrical efficiency model, both PV temperatures showed similar performance. **Conclusions:** In collectors where the PV back surface temperature is not accessible for temperature sensors mounting, the equivalent cell temperature provides a valuable alternative to be used as the PV temperature. The PV/T collector thermal and electrical performance in either closed-loop or open-loop configurations was found to be encapsulated with a series of 5 plots.

Keywords: Characterization, equivalent cell temperature, performance, PV/T collector, testing

1 Introduction

Buildings account for almost a third of the worldwide energy consumption and greenhouse gas emissions. If current trends are maintained, the International Energy Agency (IEA) estimates that the building sector energy consumption could increase by 60% from 2007 to 2050 [1]. This has resulted in an increased interest for net-zero energy buildings (NZEB) in recent years, and a number of research projects were launched on the technologies required to reach net-zero energy consumption. Combined photovoltaic/thermal (PV/T) collectors are among the technologies that are of great interest for NZEB both in residential and in commercial sectors. These collectors use PV cells as a thermal absorber and recover the heat losses from the PV to produce electricity and thermal energy simultaneously [2]. This can be done actively or passively, by a heat transfer fluid that can be either air or a liquid. Recovered heat can then be used directly in commercial buildings as pre-heated fresh air or in the case of a house, coupled with other technologies to provide domestic hot water heating or space heating.

A number of recent projects have demonstrated the potential of PV/T collectors to fulfill part of the energy requirements of buildings [3-5]. The number of products available on the market is still, however, very limited. A study conducted on the barriers of the PV/T collector market penetration [6] has shown that the absence of certification, the lack of information on their cost-benefit ratio compared to side-by-side PV and solar thermal collectors and the absence of tools to get a quick estimate of the yield of these collectors were among the reasons for the slow interest of architects and manufacturers towards this technology. In fact, even though there are standardized testing methods to characterize the performance of solar thermal collectors and PV modules, separately, there are currently no standards adapted to PV/T collectors. Manufacturers can choose the procedure used to test their products and they are not required to present their performance in any particular way. As a result, it is difficult to compare different systems and to get a quick estimate of their performance.

This study addresses some of the issues related to the thermal and electrical performance characterization of PV/T collectors. In particular, the objectives are:

- to validate the potential of the application of the equivalent cell temperature method to determine the PV cell's temperature in PV/T air collectors
- to validate models to predict the thermal performance of PV/T air collectors
- to present a graphical method to encapsulate the performance of PV/T air collectors for system design purposes

The focus is on collectors using air as the heat transfer fluid, since experience with this technology in Canada has mainly been obtained with air collectors [3-5]. Both closed-loop systems (with recirculated air) and open-loop configurations (for fresh air preheating) are considered.

To achieve these objectives, an experimental procedure with indoor and outdoor components was developed as presented in section 3. During these indoor and outdoor experiments, data was collected to obtain the parameters required to calculate the PV equivalent cell temperature as well as the collector thermal and electrical efficiencies under a wide range of conditions. The potential of using the equivalent cell temperature as the PV operating temperature in a PV/T collector was evaluated. This was achieved by developing the electrical models in section 4 using either the equivalent cell temperature or the PV back surface average temperature as the PV operating temperature and comparing their performance at predicting the PV efficiency. Then, models were developed to predict the collector thermal efficiency under quasi-stationary conditions for the collector operating in both closed-loop and open-loop conditions. Using statistical methods, the important variables in the prediction of the equivalent cell temperature and PV back surface average temperature were investigated and empirical models were developed to predict these temperatures. These models provided a link between the electrical and thermal performance of the collector which was used to develop the graphical method encapsulating the collector thermal and electrical performances.

2 Literature Review

This section presents a literature review on PV modules and solar thermal collector performance characterization standards. It also provides an overview of the work related

to PV/T collector performance characterization, highlighting the main issues with the testing of this technology.

PV Modules Standards

There are two international standards available on design qualification and type approval of PV modules: IEC 61215 for terrestrial c-Si PV modules [7] and IEC 61646 for thin film PV modules [8]. In both documents, procedures are described for module characterization and durability testing. Tests associated with the performance characterization can be performed indoors or outdoors and include the determination of the maximum power point, the temperature coefficients, the nominal operating cell temperature (NOCT) and the module performance at standard operating conditions (STC), NOCT and low irradiance.

Air Solar Thermal Collector Standards

In North America, the ANSI/ASHRAE standard 93-2010 [9] is typically used for characterizing the performance of air and liquid solar thermal collectors. For air collectors, this standard contains procedures to obtain the collector's time constant, incidence angle modifier, infiltration (or leakage) rate as a function of collector pressure and thermal performance in quasi-stationary conditions. The collector's thermal efficiency, η_{th}, is represented with the following variation of the Hottel-Whillier Bliss (HWB) equation [10]:

$$\eta_{th} = \left(\frac{A_a}{A_g}\right) F_R^{*}\left[(\tau\alpha)_e - U_L^{*}\left(\frac{T^{*}-T_a}{G}\right)\right] \quad (1)$$

In Eq. (1), A_a/A_g is the ratio of collector aperture area over the collector gross area, U_L^{*} is the collector heat loss coefficient, $(\tau\alpha)_e$ is the effective transmittance-absorptance product and $(T^{*}-T_a)/G$ is the reduced temperature. In ANSI/ASHRAE 93-2010, the fluid inlet temperature, T_i, is used as the characteristic temperature T^{*} in the calculation of the reduced temperature and thus, the heat removal factor F_R^{*} corresponds to the classical F_R coefficient of the HWB equation [10]. This is different from what is typically used in Europe for solar thermal collectors. In the European standard EN 12975-2 [11]

addressing the performance characterization of liquid solar thermal collectors, the arithmetic average fluid temperature, T_{fm}, is used as T^* along with the heat removal factor F_{AV}.

In Europe, there are no official standards to characterize the performance of solar air collectors, but a draft has been developed for non-concentrating collectors where the fluid enters and leaves the collector by only one inlet and one outlet [12]. According to this document, one of the main challenges for air solar collector characterization is that the heat transfer rate between the absorber and the heat transfer fluid is lower than in liquid collectors. As a result, the influence of flowrate on the collector's performance is greater and it is difficult to apply results obtained on a collector sample to one of greater surface area. This document has some similarities with the ANSI/ASHRAE standard 93-2010, but one main difference is the choice of T^*. The draft document [12] recommends using the fluid outlet temperature, T_o, as T^* as opposed to T_i or T_{fm}. In air collectors, T_o is close to the average collector temperature, hence it is a more logical choice for a temperature used in calculating the average loss coefficient.

PV/T Collector Characterization

There are currently no standards for characterizing or reporting on the performance of PV/T collectors. In the literature, the thermal performance of liquid PV/T collectors is often presented as a function of the reduced temperature $(T_i-T_a)/G$ [13-15]. As for the electrical performance, its dependence on irradiance and temperature cannot be captured using only the reduced temperature. In order to encapsulate the electrical performance of an open-loop air PV/T collector, Othman et al. [16] presented I-V curves for different irradiance levels at fixed flowrate and ambient temperature and the electrical efficiency for different flowrates as a function of the fluid average arithmetic temperature.

In 2003, the European initiative PV Catapult produced a guide to highlight the main issues with PV/T collector performance testing and to suggest elements to incorporate into the standards IEC 61215 [7] and EN 12975-2 [11] to address these issues. The guide focuses on non-concentrating liquid PV/T collectors using c-Si PV cells [17]. One of the

main issues discussed in this document is the fact that in a PV/T collector, the thermal performance influences the electrical performance and vice-versa. Thus, taking thermal measurements with the PV short-circuited or in open-circuit would later require the introduction of a thermal performance correction factor to account for the fact that in reality, the collector also produces electricity. PV Catapult concludes that since this factor is probably not straightforward to obtain, the PV/T collector should be producing electricity when taking thermal measurements and that it should be operating at its maximum power point. In order to save on testing time, it is further suggested that both electrical and thermal measurements be taken simultaneously by maintaining the PV at its maximum power point during thermal measurements and performing I-V curves at regular time intervals. Another issue discussed in the PV Catapult guide [17] is the feasibility of performing PV/T collector measurements indoors. Most indoor simulators used for solar thermal collector testing cannot be utilized for PV/T collectors since these usually don't have the spatial uniformity and spectral distribution required for PV testing. Similarly, the lamps used in PV testing installations are not appropriate for solar thermal collectors because these only provide a flash of light and thus, do not allow for steady-state thermal testing. As a result, PV Catapult recommends performing outdoor measurements. For glazed collectors, PV Catapult suggests taking four measurements of thermal efficiencies and reduced temperature in steady-state conditions for four different average fluid temperatures, T_{fm}, in order to obtain 16 measurement points. For unglazed collectors, three temperature values T_{fm} at three different wind speeds are recommended for a total of 9 measurement points. The models suggested to characterize the performance are those of EN 12975-2 for liquid solar thermal collectors. These models have a higher level of complexity than the HWB model since for glazed collectors, a second order term is added to take the non-linearity of thermal losses into account and in the case of unglazed collectors, wind dependency terms are incorporated. For the electrical measurements, PV Catapult suggests obtaining instantaneous maximum power point measurements through current-voltage (I-V) tracing in order to fill out a matrix with 100 W/m^2 irradiance bins and 5°C temperature bins in a minimum span of 30°C. Considering that the PV temperature cannot necessarily be measured, the draft states that the temperature used in the thermal bins should have a direct relation with the actual PV

temperature so that the latter can be calculated during the data analysis from the measured temperature, weather and collector thermal performance.

As part of the International Energy Agency Solar Heating and Cooling Program (IEA SHC) Task 35 "PV/Thermal Solar Systems" [18], a report was produced to suggest three types of characterization schemes for PV/T collectors with different levels of detail for design, rating and marketing purposes [19]. The PV/T collector design scheme concept developed consists of a 3-plot system with a 1st plot presenting the thermal performance as a function of the reduced temperature, a 2nd plot showing the link between the reduced temperature and $(T_{PV}-T_a)/G$ and finally, a 3rd plot expressing $(T_{PV}-T_a)/G$ as a function of the electrical efficiency for various ambient temperatures. This scheme has great potential to be used for design purposes or for performance comparison between different collectors since both the thermal and electrical efficiencies can be obtained by navigating from one plot to another without having to perform any calculations. It has some limitations, however, because it only applies to a particular flowrate and wind speed and additionally, in the case of the 3rd graph, to a single inlet temperature.

Summary

This review shows that the variables affecting the thermal and electrical performance of solar thermal collectors and PV modules operating separately are known, but that it is not clear how the interaction between the electrical and thermal yields can be encapsulated in the performance characterization of combined PV/T collectors. As mentioned by PV Catapult [17], one way to relate both aspects could be to link the PV temperature to the collector thermal performance. Finding a relation between the two is a challenge, however, because the PV temperature in a PV/T collector is difficult to measure. This is not only due to the temperature non-uniformity, but also to the fact that the back of the cells in such collector is not always accessible for sensor mounting. Thus, since it is not clear how this temperature can be measured, it is also not straightforward to determine how it can be predicted from the weather and collector operating conditions, an essential piece of information to link the electrical and thermal performance and obtain simple performance prediction models that can be used for design purposes.

3 Methodology

The experimental procedure developed consists of two parts: an indoor procedure to obtain particular electrical parameters and an outdoor procedure to acquire measurements to fully characterize the collector thermal and electrical performance. The experiment was carried out on two unglazed PV/T collector modules having a total gross area of 3.513 m^2 with an absorber consisting of monocrystalline-silicon (c-Si) cells.

Indoor Testing Procedure

The indoor test aimed at obtaining the thermal diode voltage factor, *D*, and the open-circuit voltage temperature coefficient, $\beta_{Voc,}$ two parameters that are essential in the calculation of the equivalent cell temperature, *ECT*. This *ECT* is the temperature at which the PV cells operate. According to the standard IEC 60904-5 [20] containing the detailed procedure on how to obtain this temperature, the *ECT* can be calculated with Eq. (2) assuming the open-circuit voltage and irradiance are known variables.

$$ECT = T_{PV,1} + \frac{1}{\beta_{Voc}}\left[V_{oc} - V_{oc,1} + DNs \ln\left(\frac{G_1}{G}\right)\right] \tag{2}$$

In Eq. (2), V_{oc} is the open-circuit voltage, and *Ns* is the total number of cells in series in the PV array. The subscript *1* refers to the reference observation for which the PV temperature is known. The coefficient β_{Voc} is evaluated with open-circuit measurements obtained at different temperatures, but constant irradiance levels. As for the parameter *D*, it is calculated with two open-circuit voltages measured at the same PV temperature, but different irradiance conditions, G_3 and G_4, using Eq. (3).

$$D = \frac{1}{Ns}\frac{V_{oc4} - V_{oc3}}{\ln\left(G_4 / G_3\right)} \tag{3}$$

The tests required for the calculation of the parameters *D* and β_{Voc} are performed indoors, because these require that the PV temperature be kept uniform, and varied within a 30°C temperature range. In theory, this uniform temperature could be achieved outdoors with a PV/T collector under stagnation conditions, i.e. with no flow in the collector. In outdoor

and stagnation conditions, however, the temperature inside the collector cannot be controlled. Thus, obtaining measurements in a large PV temperature range is difficult in a limited time frame.

This indoor test was performed with a Class B large area pulsed solar simulator located in an environmental chamber. Only one of the two PV/T modules was used because of space limitations. The irradiance was measured with a monocrystalline reference cell and the PV temperature was obtained with 6 thermocouples mounted at different locations at the back surface of the cells. The temperature coefficients were determined with sets of measurements taken at 7 different average back surface temperatures ranging from 10 to 36°C at an irradiance of 1000 W/m^2. As for the thermal diode voltage, it was determined from I-V curves taken with the PV back surface average temperature constant at 25°C at 5 irradiance levels varying from 200 W/m^2 to 1000 W/m^2. For each measurement, the room was heated or cooled until all PV back surface measurements were stable. Then, the irradiance was set to the desired level using crystalene sheets having the capability of varying the irradiance without affecting the spectrum. Finally, an I-V curve was traced while the collector was flashed with the lamp, and both the back surface PV module temperatures and reference cell short-circuit current were recorded. A total of three I-V curves were obtained for each set of conditions.

Outdoor Testing Procedure

The objective of the outdoor test was to gather sufficient data to characterize the collector thermal and electrical performance in open-loop and closed-loop configurations at normal incidence angle. To obtain these measurements, the two collectors were mounted in series on a zenith-azimuth tracking testing rig. Two collectors were used so that the area would be greater than 3 m^2 as recommended in the draft standard for solar air heaters [12]. The two collectors were mounted in a building-integrated configuration, a typical mounting configuration for residential buildings. This was done by adding 25.4 mm of Styrofoam board insulation with a corresponding thermal resistance of 0.88 m^2·K/W to the collector rear and side surfaces. The collector was instrumented according to the recommendations

of the ANSI/ASHRAE standard 93-2010 as shown in Fig. 1. Blowers were mounted at both collector inlet and outlet to regulate the pressure inside the collector.

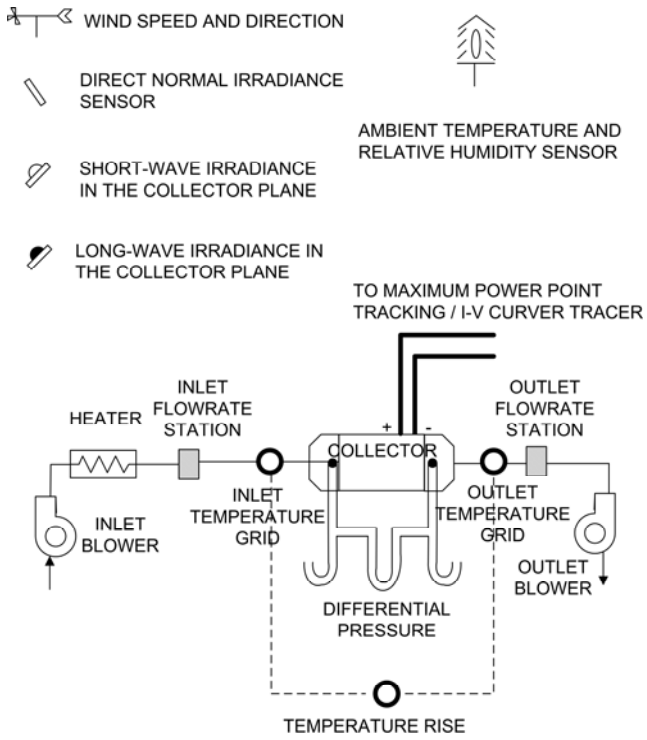

Figure 1 PV/T collector testing loop schematic

The inlet temperature and temperature rise measurements were done with type-T thermocouple grids located at the collector inlet and outlet. Each thermocouple grid consisted of a total of 12 thermocouples located in the middle of concentric circles of equal cross sectional areas as recommended in the ANSI/ASHRAE standard 93-2010 [9]. The pressure measurements were obtained with pressure taps located in the collector transition elements and a pressure transducer with digital output. Inlet and outlet flowrates were measured with differential pressure flow sensors. The in-plane short-wave and long-wave irradiance as well as the direct normal irradiance were measured with a pyranometer, pyrgeometer and pyrheliometer, respectively. The outdoor temperature and relative humidity were obtained with a humidity and temperature transmitter and the 10 m wind speed and direction were measured with a propeller-type anemometer. The data measured by the sensors located on the testing rig were recorded at a 5 second time interval with a data acquisition system. As for the output signals of the wind, direct

normal irradiance, ambient temperature and relative humidity sensors, these were recorded at a 1 minute time interval.

The collector was connected to a device that allowed continuous operation at maximum power point through a charge controller with a quick manual bypass to an I-V curve tracer. The PV back surface temperature was measured with 6 equidistant type-T thermocouples located at the back of the cells and was recorded at a 10 second time interval. The collector mounted on the testing rig for the combined electrical and thermal testing is shown in Fig. 2.

Measurements were obtained for 9 different conditions consisting of the combinations of 3 fluid inlet temperatures (T_a, 40°C and 44°C) and three inlet flowrates (40, 55, 75 kg/(h·m^2)). During measurements, normal incidence angle was maintained by varying the slope and azimuth angle of the collector. I-V curves were traced at 2 to 4 minute time intervals. For a measurement to be considered valid, quasi-stationary conditions had to be maintained for at least 45 minutes. The first 30 minutes consisted of the preconditioning phase and every subsequent 15 minute period was considered as a measurement phase. This 15 minute period was then sub-divided in three measurements of 5 minute. During this whole period (preconditioning and measurement), the fraction of diffuse radiation had to be less than 30% of the irradiance. Moreover, the in-plane irradiance had to be greater than 700 W/m^2, with a maximum deviation of ±50 W/m^2. The other maximum deviations allowed were set at ±20 W/m^2 for the long-wave irradiance, ±5% for both the inlet and outlet flowrates and ±1 K for the inlet and ambient temperatures. In addition to the combined electrical and thermal measurements, data under stagnation conditions were also collected. During stagnation, normal incidence angle was still maintained, but the air heating apparatus and inlet and outlet blowers were turned off.

Figure 2 PV/T collector mounted on the outdoor combined PV and thermal testing rig

4 Results

Electrical Model Validation

The parameter β_{Voc} was obtained with the data collected during the indoor test by performing a linear regression on V_{oc} as a function of $T_{PV\_back,AVG}$ at 1000 W/m^2. The slope of this linear regression corresponds to β_{Voc} and was found to be -(0.118 ± 0.001) V/°C with a correlation coefficient, R^2, of 0.99 where R^2 is defined in Appendix A. Using Eq. (3), a thermal diode voltage of (0.0320 ± 0.0007) V was calculated.

The coefficients of the electrical models to predict the electrical performance were obtained using either the *ECT* or $T_{PV\_back,AVG}$ as the PV temperature, where $T_{PV\_back,AVG}$ is the average of the temperature measurements taken at the back surface of the PV cells. The *ECT* was calculated for the outdoor measurements collected during the combined electrical and thermal testing using Eq. (2). The reference observation in Eq. (2) was selected from the dataset collected during the outdoor testing. In order to ensure that the average of the temperature measurements taken at the back of the PV cells was representative of the equivalent operating cell temperature, this observation was taken

when the collector was under stagnation and quasi-stationary conditions and all T_{PV_back} measurements were within 3°C.

The PV maximum power point as a function of $T_{PV\_back,AVG}$ and *ECT* for the outdoor observations is presented in Fig. 3 (a) and (b), respectively.

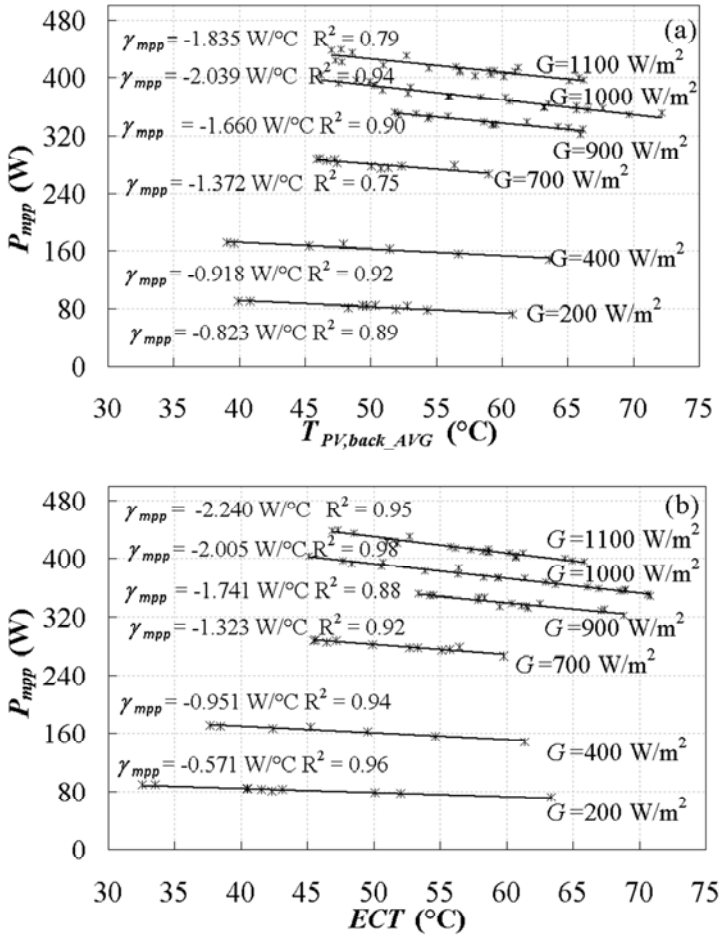

Figure 3 PV maximum power point for various irradiance levels as a function of (a) $T_{PV\_back,AVG}$ (b) *ECT*

These graphs contain the information to identify the PV efficiency at the reference temperature for a number of irradiance levels, $\eta_{mpp}(G, T_{ref})$, as well as the relative maximum power point temperature coefficient as a function of irradiance, $\gamma_{mpp,rel}(G)$. With this information, the PV efficiency at any given temperature and irradiance level, $\eta_{mpp}(G, T_{PV})$, can be computed by using:

$$\eta_{mpp}(G,T_{PV}) = \eta_{mpp}(G,T_{PV,ref}) * \left(1 + \gamma_{mpp,rel}(G) * \left(T_{PV} - T_{PV,ref}\right)\right) \quad (4)$$

Usually, $T_{PV,ref}$ in Eq. (4) is 25°C, but in this case, the ambient temperature did not allow PV measurements below 30°C. As a result, $T_{PV,ref}$ was set at 55°C. The performance of the model shown in Eq. (4) using either $T_{PV\_back,AVG}$ or ECT as T_{PV} was tested against electrical measurements obtained under both stagnation and heat recovery conditions. As model performance indicators, the following statistical indices defined in Appendix A were used: mean bias error (MBE), root mean square error (RMSE) and correlation coefficient (R^2). The comparison of the model performance at predicting η_{mpp} using ECT and $T_{PV\_back,AVG}$ is shown in Table 1. The errors are small in both cases since the MBE and RMSE are under 0.3% and 1.6% for both temperatures and the R^2 is above 0.93.

Table 1 Comparison of the electrical efficiency model performance using $T_{PV}=T_{PV\_back,AVG}$ and $T_{PV}=ECT$

T_{PV}	MBE	MBE (%)	RMSE	RMSE (%)	R^2
$T_{PV\_back,AVG}$	-0.0003	-0.28	0.0017	1.59	0.93
ECT	0.0002	0.18	0.0012	1.07	0.97

Thermal Performance Model Validation for Closed-Loop Collectors

With the data collected during the outdoor experiment, the thermal efficiency of this air PV/T collector was computed using Eq. (5).

$$\eta_{th} = \frac{c_p\left(m_o T_o - m_i T_i - m_L T_a\right)}{G A_g} \tag{5}$$

In Eq. (5), the effect of temperature on air properties is neglected and as a result, the air thermal capacity, c_p, is assumed to be constant. A_g is the collector gross area, m_o and m_i are the outlet and inlet air flowrates and m_L is the air leakage rate taken as a positive value for infiltration and a negative value when leakage occurs.

The thermal efficiency as a function of the reduced temperatures $(T_i-T_a)/G$, $(T_o-T_a)/G$ and $(T_{fm}-T_a)/G$ is shown in Fig. 4 where each point represents one of the three 5 minute averages of the 15 minute measurement period. These graphs include data taken at two flowrates, three inlet temperatures and an average wind speed of (0.9 ± 0.3) m/s. The uncertainty bars on this plot and on all subsequent plots represent the expanded

uncertainty for a confidence level of 95%. The method employed for the calculation of the uncertainties is presented in Appendix B. Figure 4 shows that the thermal efficiency decreases with the increase of reduced temperature, but increases with the increase of flowrate.

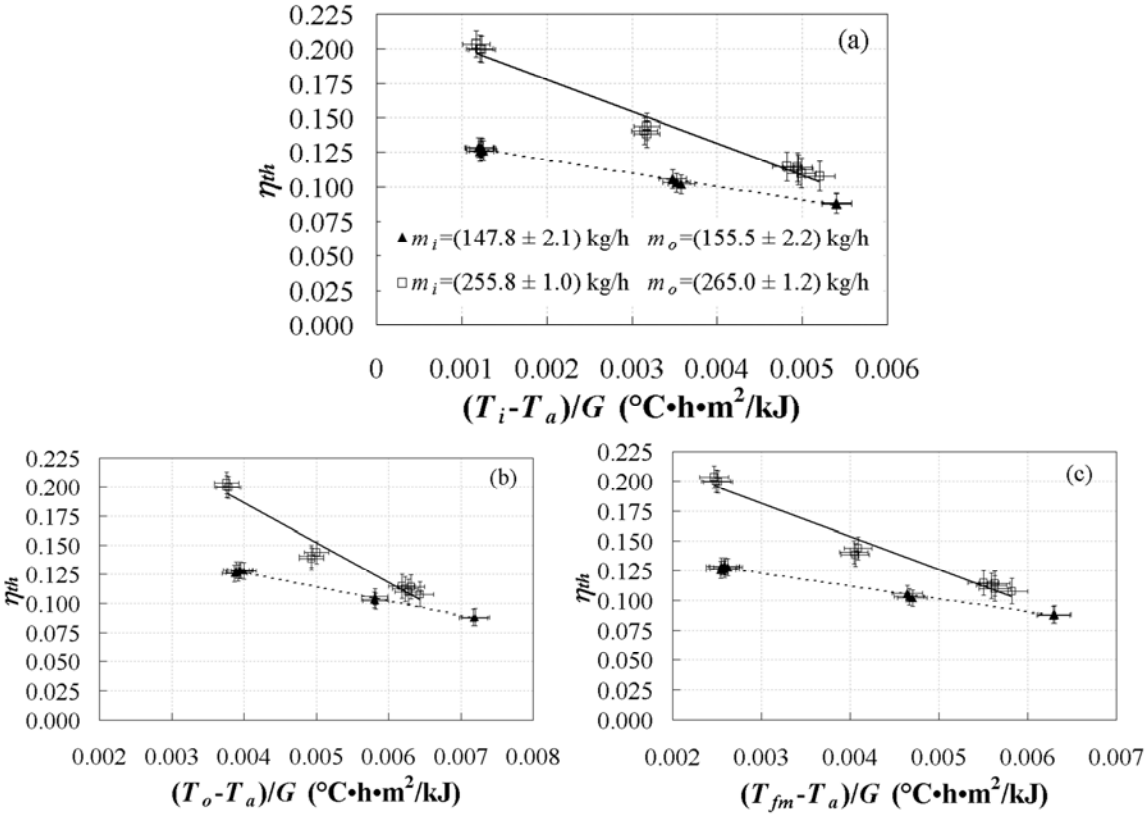

Figure 4 Thermal efficiency in closed-loop as a function of (a) $(T_i-T_a)/G$ (b) $(T_o-T_a)/G$ (c) $(T_{fm}-T_a)/G$

By performing a simple linear fit for each flowrate of Fig. 4, the coefficients of the model shown in Eq. (6) can be obtained.

$$\eta_{th} = \overline{F_R^*(\tau\alpha)_e} - \overline{F_R^* U_L^*}\left(\frac{T^* - T_a}{G}\right) \tag{6}$$

In Eq. (6), $\overline{F_R^*}$ is the PV/T collector heat removal factor, $\overline{(\tau\alpha)_e}$ is the PV/T collector effective transmittance-absorptance product, and $\overline{U_L^*}$ is the overall PV/T collector heat loss coefficient. When $T^*=T_i$, this model corresponds to the Hottel and Whillier equation modified by Florschuetz [21] for PV/T collectors. The difference between the solar thermal and PV/T collector models resides in the bars added above F_R^*, $(\tau\alpha)_e$ and U_L^*

indicating that these variables are affected by the electrical performance. Table 2 presents the model coefficients for the three T^* considered. The high R^2 values obtained for each temperature show that this model not only represents well the thermal performance of this PV/T collector, but also that all three temperatures can be used as T^* without any significant effect on the model performance.

Table 2 Thermal efficiency model coefficients

	m_i=(147.8 ± 2.1) kg/h m_o=(155.5 ± 2.2) kg/h			m_i=(255.8 ± 1.0) kg/h m_o=(265.0 ± 1.2) kg/h		
	$T^*=T_i$	$T^*=T_o$	$T^*=T_{fm}$	$T^*=T_i$	$T^*=T_o$	$T^*=T_{fm}$
$\overline{F_R^*(\tau\alpha)_e}$	0.139	0.176	0.155	0.233	0.323	0.264
$\overline{F_R^* U_L^*}$	9.713	12.318	10.865	23.442	34.194	27.675
R^2	0.99	0.99	0.99	0.97	0.95	0.96

Thermal Performance Model Validation for Open-Loop Collectors

With the collected data in open-loop configuration, i.e. drawing air directly from ambient without using the air heating unit, the range of reduced temperature is too small to detect any relation between η_{th} and $(T^*-T_a)/G$. As a result, a model of the thermal efficiency as a function of a reduced temperature does not make sense for open-loop collectors. As shown in Fig. 5, a representation of the thermal efficiency as a function of the outlet flowrate is more appropriate. These observations can be fit with a 2nd degree polynomial.

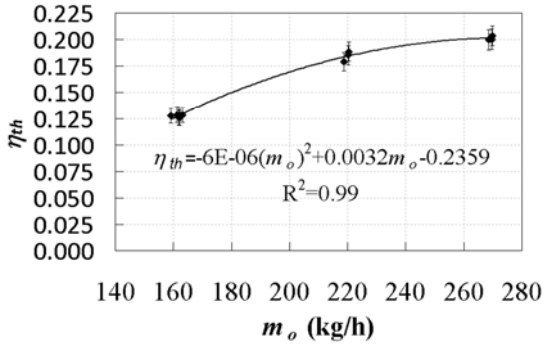

Figure 5 Thermal efficiency in open-loop as a function of the outlet flowrate

PV Cell's Temperature Prediction Model Validation

The Pareto diagrams in Fig. 6 present the *t-value* of the different variables potentially influencing $T_{PV\_back,AVG}$ and *ECT* when air is circulating in the collector. The fluid average

temperature, T_{fm}, is not included in these plots since it can be calculated from T_i and T_o. From this figure, it can be observed that the main variable influencing both *ECT* and $T_{PV\_backAVG}$ is the fluid outlet temperature, T_o. The second and third most important variables are G and T_i for the *ECT* and T_i and G for the case of $T_{PV\_back,AVG}$. Considering a *p-value* of 0.05 as the threshold chosen for statistical significance, the fluid inlet and outlet flowrates can be considered as not statistically significant variables in this case. The wind speed, V_w, and the ambient temperature, T_a, are statistically significant variables, but are not as important as T_o, G and T_i.

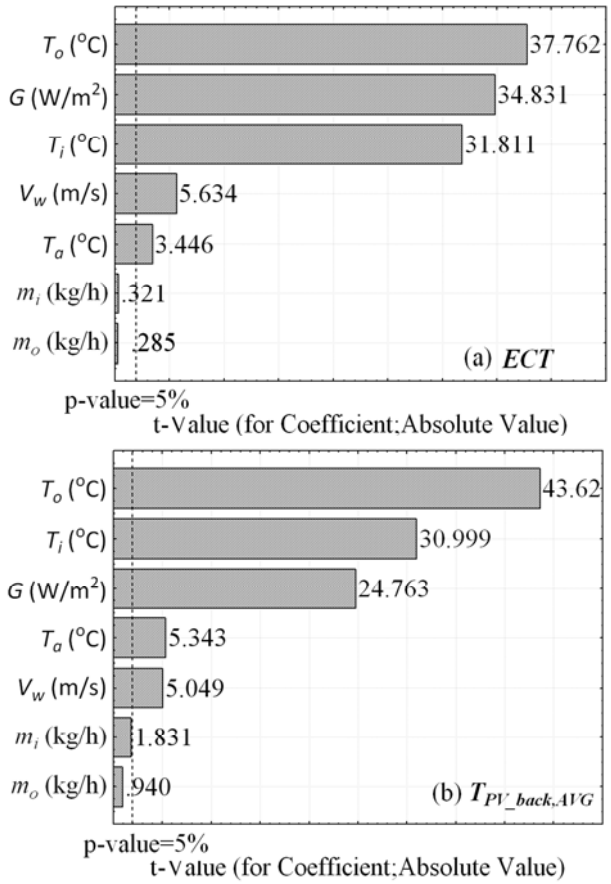

Figure 6 Pareto diagrams identifying the most important variables in the prediction of (a) *ECT* and (b) $T_{PV\_back,AVG}$

The electrical measurement dataset obtained under heat recovery conditions was randomly split into train and test datasets to first develop the model and then evaluate its performance. A comparison of the performance of some of the models investigated using selection of variables methods is shown in Table 3. This table only presents first order

multiple linear regression models, but higher order models were also investigated as well as exponential models. A 3-variable multiple linear regression model was found to be sufficient using the variables T_i, T_o and G.

Table 3 Model performance comparison at predicting T_{PV}

	ECT			$\boldsymbol{T_{PV\_back,AVG}}$		
Variables in multiple linear regression	**MBE (%)**	**RMSE (%)**	**R^2**	**MBE (%)**	**RMSE (%)**	**R^2**
G, T_i, V_w, T_{fm}	-0.21	4.52	0.92			
G, T_i, T_{fm}	-0.27	4.60	0.91	-0.08	3.77	0.92
G, T_o, T_i	-0.27	4.60	0.91	-0.09	3.77	0.92
G, T_o, T_{fm}	-0.27	4.60	0.91	-0.08	3.77	0.92
T_o, T_i	0.69	8.30	0.72			
G, T_o, m_i, T_{fm}				-0.22	3.56	0.93
T_i, T_{fm}				0.45	5.60	0.82
G, T_o, T_i, $\ln(T_a)$				-0.12	3.75	0.92

A residual analysis of this model conducted with both $T_{PV\_back,AVG}$ and *ECT* confirmed the validity of the model with the residuals following a normal distribution and not showing any trend with the model variables. The final models and their performance at predicting T_{PV} after this residual analysis and the removal of outliers are shown in Table 4. In the case of the *ECT*, this model does not have any intercept, because it was not found to be statistically significant. From this table, it can be concluded that both models have very similar performance at predicting T_{PV} with a R^2 of 0.937 in the case of $T_{PV\_back,AVG}$ and 0.941 for the *ECT*.

Table 4 Multiple linear regression model performance at predicting T_{PV}

Coefficients	$\boldsymbol{T_{PV\_back,AVG}}$	***ECT***
Intercept	4.426	-
$\boldsymbol{T_o}$ **(1/°C)**	1.867	2.127
$\boldsymbol{T_i}$ **(1/°C)**	-0.937	-1.234
$\boldsymbol{G}$ (m^2/W)	0.008	0.015
Performance Indicator		
MBE	-0.063	-0.158
MBE (%)	-0.109	-0.269
RMSE	1.855	2.178
RMSE (%)	3.225	3.715
R^2	0.937	0.941

Table 5 presents the performance of the model shown in Eq. (4) at predicting η_{mpp} when T_{PV} is calculated using the 3-variable multiple linear regression model coefficients of Table 4. According to these results, using *ECT* as T_{PV} in the case of this PV/T collector is comparable to using the average PV back surface temperature over the whole PV electrical efficiency range. As shown in Fig. 7, the predictions using $T_{PV\_back,AVG}$ are better at low efficiency levels, while those using the *ECT* perform better at high efficiency levels.

Table 5 Comparison of the PV electrical efficiency models performance using T_{PV} calculated by the 3-variable multiple linear regression models of Table 4

T_{PV}	MBE	MBE (%)	RMSE	RMSE (%)	R^2
$T_{PV\_back,AVG}$	0.000	-0.247	0.002	1.766	0.903
ECT	0.000	0.146	0.002	1.598	0.920

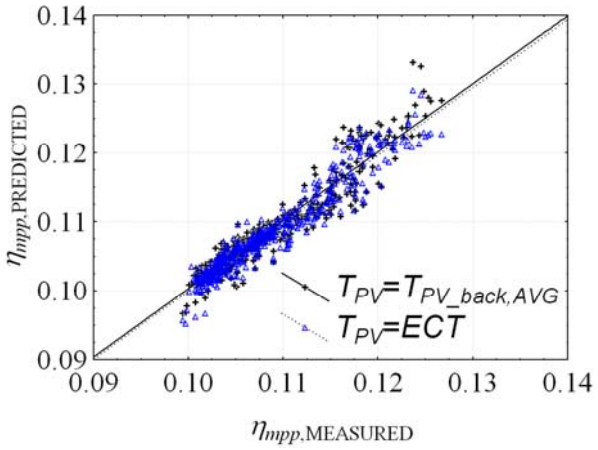

Figure 7 Comparison of the measured and predicted electrical efficiencies using T_{PV} calculated with the 3-variable multiple linear regression model

PV/T Model Development for Design Purposes

The models obtained for closed-loop collectors allow the computation of the PV/T collector thermal efficiency from the reduced temperature $(T^*\text{-}T_a)/G$ and flowrate. The electrical model expresses the electrical efficiency as a function of the irradiance and PV cell's temperature. This temperature can be estimated with models using the irradiance and fluid inlet and outlet temperatures as independent variables. These models can be presented in a 5-plot system that captures the collector performance. These 5-plot systems are applicable at the collector gage pressure and wind speed range under which they were developed. They are also only valid for the building-integrated configuration

considered here since the thermal efficiency and PV temperature models would not necessarily remain identical if the collector back and edges were poorly insulated.

The 5-plot system for the open-loop configuration is presented in Fig. 8. The 1st plot presents the thermal efficiency as a function of the outlet flowrate obtained from experimental data. This first graph represents actual experimental data and extrapolation of the thermal efficiency curve should be avoided. In the 2nd graph, the temperature rise is plotted as a function of the outlet flowrate and irradiance. The curves on the 2nd plot are obtained using the measured thermal efficiency and outlet flowrate for irradiance levels varying from 200 W/m^2 to 1000 W/m^2 with steps of 200 W/m^2 using the following equation:

$$\frac{\eta_{th} G A_g}{m_o c_p} = T_o - T_i = T_{rise} \tag{7}$$

This temperature rise can be used in the 3rd plot to obtain the fluid outlet temperature for various ambient temperatures. This plot is not specific to this collector, but is simply used here to simplify going from one plot to another. The ambient temperature curves are selected to be representative of the ambient temperature range under which the collector is meant to operate even though interpolation is allowed. In the 4th plot, the PV temperature can be estimated since it is presented as a function of the fluid outlet temperature for various irradiance levels. The influence of the fluid inlet temperature is neglected because this last variable was found to be the least significant in the model to predict T_{PV}. This PV temperature can be used in the 5th plot to estimate the PV maximum power point. Plots 4 and 5 are produced from the models developed to predict the PV temperature and the PV power production. The ranges used for the fluid outlet temperature, PV temperature and electrical power production should correspond to those typical of the collector operation.

The method for using these plots can be illustrated with the following example represented with dotted lines in Fig. 8. Assuming an outlet flowrate of 200 kg/h, an irradiance of 1000 W/m^2 and an ambient temperature of 20°C, the 1st and 2nd plots

indicate that the thermal efficiency is 0.164 and the temperature rise is 10°C. Using this temperature rise in the 3rd plot, we get that T_o is 30°C. With T_o, an estimate of 54°C for T_{PV} is obtained in the 4th plot. This leads to a maximum power point of 385 W in the 5th plot. The estimates for T_{PV} and P_{mpp} with the 5-plot system are closed to the actual values calculated by the models when the fluid inlet temperature effect on the temperature of the PV cells is included. Using the actual models instead of plots 4 and 5, values of 54.1°C and 284.3 W are obtained for T_{PV} and P_{mpp}, respectively.

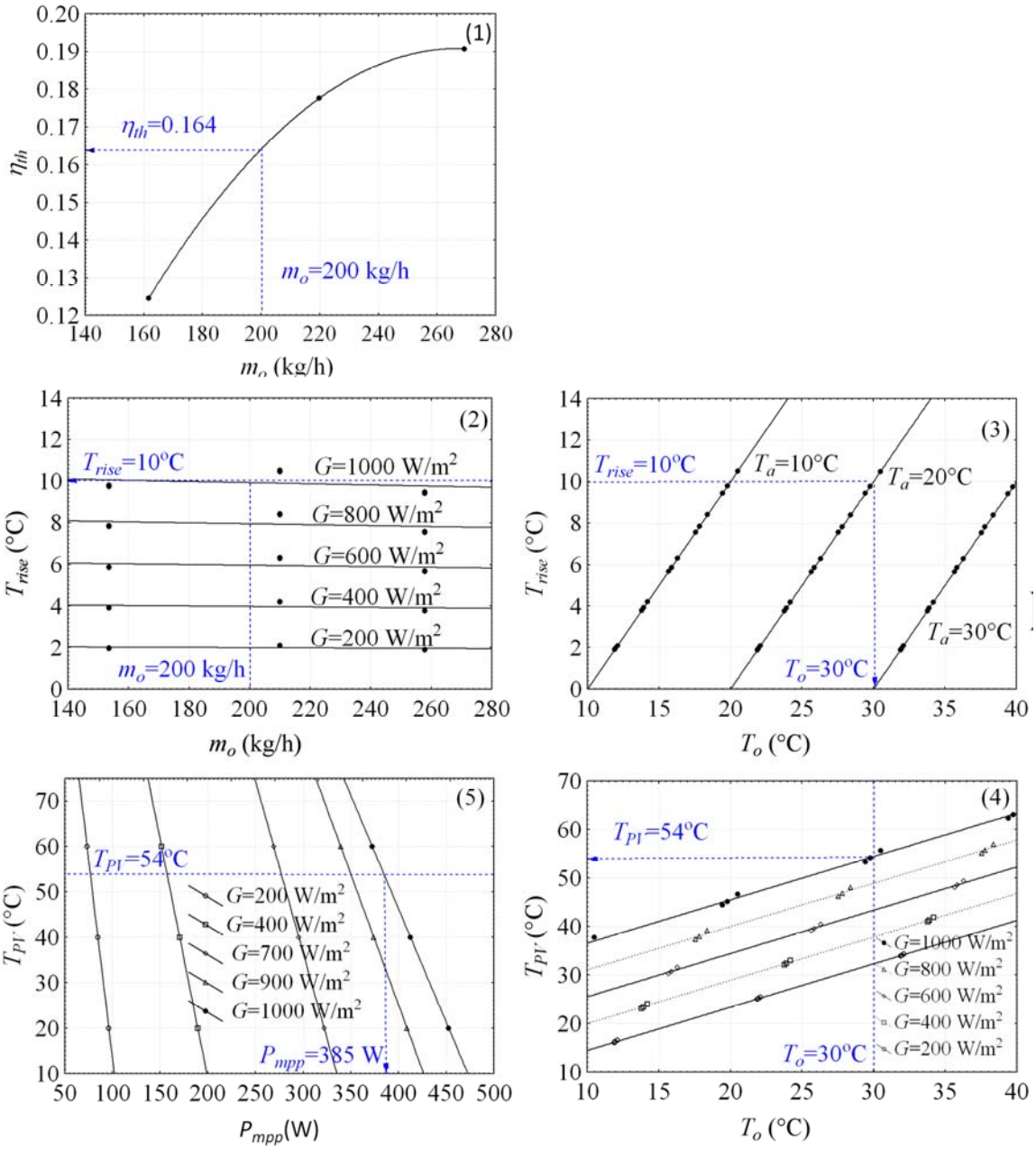

Figure 8 5-plot system representing the PV/T collector performance in open-loop configuration

The 5-plot system for the closed-loop collector presented in Fig. 9 takes into account the fact that the air infiltrating the collector or leaking from the collector is not always at the same temperature as the air entering the collector through the actual inlet. In this case, the collector thermal efficiency can be expressed as a function of an effective inlet temperature, $T_{i,eff}$, with the following relation:

$$\eta_{th} = \frac{m_o c_p \left(T_o - T_{i,eff}\right)}{GA_g} \tag{8}$$

In Eq. (8), T_o-$T_{i,eff}$ is the effective air temperature rise $T_{rise,eff}$ where the effective inlet temperature, $T_{i,eff}$, is defined as:

$$T_{i,eff} = \frac{m_i T_i + m_L T_a}{m_o} \tag{9}$$

In Fig. 9, the 1st plot presents the thermal efficiency as a function of the reduced temperature. In this case, T_i is the preferred characteristic temperature T^* since T_i is the only known variable at the design stage considering that T_o and T_{fm} are both obtained from the actual collector performance. Similar to the 1st plot of the open-loop configuration, this graph is produced from experimental data. Thus, neither interpolation between curves nor extrapolation should be performed. The 2nd graph presents the effective air temperature rise, $T_{rise,eff}$, as a function of $m_o c_p/(GA_g)$. It is produced using Eq. (8) with measured minimum and maximum thermal efficiencies, a single inlet and ambient temperature and irradiance levels varying from 200 to 1000 W/m^2. Interpolation between the curves should not occur because the variation of the effective temperature rise is not linear with $m_o c_p/(GA_g)$. The 3rd plot is obtained with the data used for the 2nd plot, but in addition, calculations are made for the full inlet temperature range. The last two graphs are identical to those of the open-loop configuration.

An example is shown on this graph for a collector having the following operating conditions: m_i=147.8 kg/h, T_i=30°C, T_a=20°C and G=1000 W/m^2. For a collector

operating under the same gauge pressure as during testing, the fluid outlet flowrate is 155.5 kg/h and $T_{i,eff}$ is estimated at 29.5°C. With calculated values for $(T_i\text{-}T_a)/G$ and $m_o c_p/(GA_g)$ of 0.0028 (°C·h·m^2)/kJ and 0.0123 °C^{-1}, respectively, the first plot indicates that the thermal efficiency is 0.11. Using η_{th} in the second plot, $T_{rise,eff}$ is found to correspond to 9°C. From this 2nd plot, moving to the 3rd, 4th and 5th plots allows the estimation of T_o (38.5°C), T_{PV} (62°C) , and P_{mpp} (367.5 W). Using the actual models instead of plots 4 and 5, values of 59.9°C and 373 W are obtained for T_{PV} and P_{mpp}, respectively.

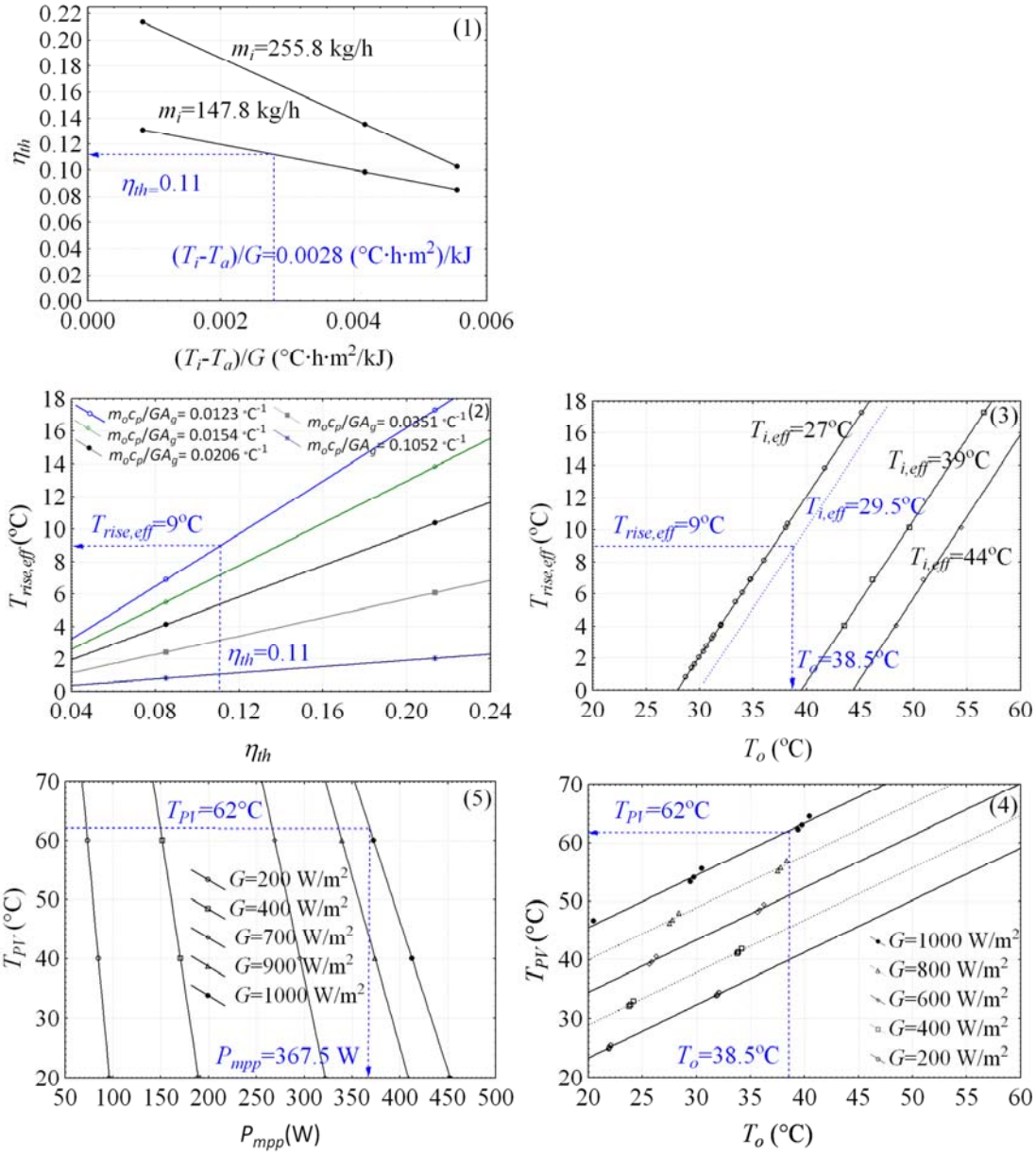

Figure 9 5-plot system to represent the PV/T collector in closed-loop

5 Discussion

In a PV/T collector, the channels or tubes behind the PV cause the electrical performance characterization to be somewhat of a challenge. One of the reasons is that the heat transfer fluid harvesting the heat from the PV causes the cells to be at a non-uniform temperature. For cells mounted in series, the PV will operate at the average cell temperature. Thus, the measurement of the true average PV cell's temperature requires the mounting of multiple temperature sensors. This is feasible in theory, but in reality, in most PV/T collectors, it is difficult to access the back-surface of the PV cells. The equivalent cell temperature method has great potential for modeling the PV operating temperature, since it does not require any temperature measurements and only the open-circuit voltage needs to be recorded. It has the only disadvantage of requiring indoor testing to obtain the thermal diode voltage factor and open-circuit voltage. In theory, these two variables can be obtained outdoors, but obtaining a uniform temperature for the PV cells outdoors in a PV/T collector is a challenge and might be time consuming.

Figure 10 presents the collector performance in closed-loop configuration according to the 3-plot design scheme concept developed by the IEA [19]. This 3-plot system differs slightly from the original design scheme developed by the IEA, however, because the 2nd plot includes a categorization with regards to the ambient temperature. Using the same example than in section 4, we find in the 2nd plot that $(T_{PV}\text{-}T_a)/G$ corresponds to 0.011 (°Chm^2)/kJ for a reduced temperature of 0.0028 (°Chm^2)/kJ. In the 3rd plot, $(T_{PV}\text{-}T_a)/G$ is used to obtain a PV efficiency of 0.11. Thus, according to this design scheme, the maximum power point is estimated at 386 W which is acceptable since it is within 3.5% of the value obtained with the actual models. This error is slightly greater than the 1.5% obtained with the 5-plot system in section 4. Thus, in this case, the 5-plot offers a limited improvement in accuracy and is also restricted to one wind speed and operating pressure. The 5-plot system is valid at multiple flowrates, however, and it can be applied to both open-loop and closed-loop configurations. These are two significant advantages compared to the 3-plot system.

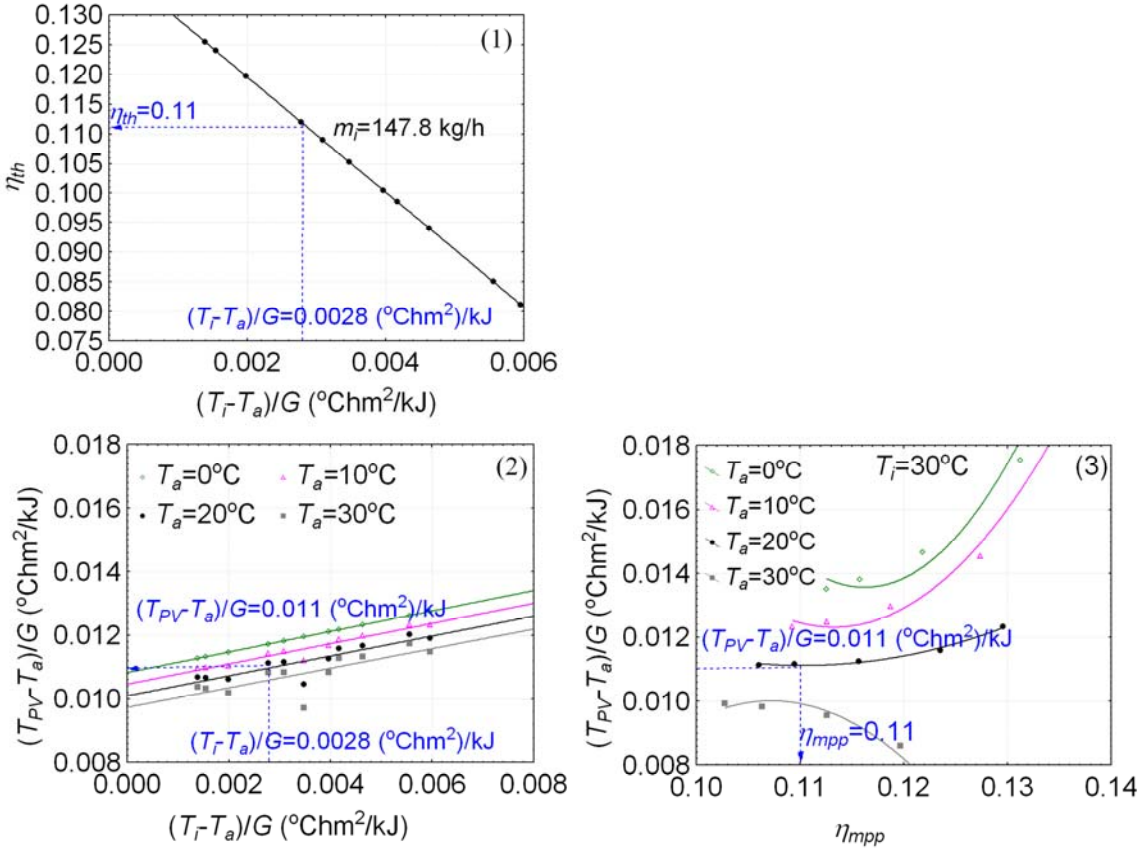

Figure 10 3-plot system adapted from the IEA to represent the PV/T collector in a closed-loop configuration

Some aspects of PV/T air collector performance are still unknown, however, such as the effect of slope on the collector performance and the validity of these schemes for collectors of different areas and module configurations (series vs parallel). Another important aspect of PV/T collectors is that these often operate under stagnation conditions. Models to predict the PV temperature using either the *ECT* or the back surface average temperature must also be developed for such operating conditions.

The collector studied here was found to have a relatively low thermal efficiency. The focus of this study, however, is not on the actual PV/T collector performance and coefficients obtained in the different models, but on the method used to fully characterize the thermal and electrical yield of this technology. This method could be applied to different types of PV/T air collectors to simplify the comparison of different designs.

6 Conclusions

Standardized methods to test, characterize and present the performance are important for every technology since these enable comparisons between different products and the development of simplified models to predict their yield. This study presented a characterization method and a 5-plot system applicable for design calculations of open-loop and closed-loop air PV/T collectors in a building-integrated configuration.

An important finding of this study is related to the PV temperature measurement and to its linkage with the collector thermal yield which has been an issue for the characterization of PV/T collectors. It was found that the use of the equivalent cell temperature as the PV operating temperature provided comparable results to the use of the average PV back surface temperature for predicting the collector electrical efficiency. An investigation of the important variables in the prediction of the PV temperature showed that a multiple linear regression model using the fluid inlet temperature, the irradiance and the fluid outlet temperature as independent variables could be used successfully to estimate both the PV back surface average temperature and equivalent cell temperature. When using the *ECT* and the PV back surface average temperature calculated with these models to compute the electrical efficiency, similar results were obtained. Nevertheless, the use of the *ECT* as opposed to $T_{PV\_back,AVG}$ provides a valuable alternative for PV/T collector characterization, for example in collectors where the PV back surface temperature is difficult to access for temperature sensor mounting or where measurement could affect the air flow in the channel. It does require the open-circuit voltage to be known, but I-V curves need to be traced for the electrical characterization. The thermal efficiency models using the inlet, outlet or average fluid temperature in the calculation of the reduced temperature had similar performance. Considering that the fluid inlet temperature is the only known temperature at the design stage, it was concluded that the use of this temperature made more sense for closed-loop collectors. For the collector tested in an open-loop configuration, the reduced temperature variation was found to be too small to detect any relation with the thermal efficiency. Thus, a model of the thermal efficiency as a function of the fluid outlet flowrate was found to be more appropriate.

From these models characterizing thermal and electrical performance, and the relation between the thermal and electrical yields, two series of graphs were developed for both closed-loop and open-loop configurations to encapsulate all the collector performance characteristics. These series consist of 5-plot systems that can be used for design purposes to estimate the thermal efficiency, the air temperature rise, the PV temperature and the PV electrical production from the weather and collector operating conditions.

Acknowledgements

Financial support for this project was provided by the ecoENERGY Technology Initiative (ecoETI), a federal program led by Natural Resources Canada aiming towards greenhouse gas emissions reduction and clean air. The authors would like to acknowledge Yves Poissant and Dave Turcotte for their contribution on the development of the experimental procedure. The outdoor experimental measurements were performed at Canada's National Solar Testing Facility (Alfred Brunger).

Nomenclature

Symbols

A	Area (m^2)
c_p	Air specific heat (kJ/(kg·°C))
F_R*	Heat removal factor with characteristic temperature T* in reduced temperature for solar thermal collectors
$\overline{F_R}$*	Heat removal factor with characteristic temperature T* in reduced temperature for PV/T collectors
F_R	Heat removal factor with the fluid inlet temperature used as the characteristic temperature in the calculation of the reduced temperature for solar thermal collectors
F_{AV}	Heat removal factor with the average fluid temperature used as the characteristic temperature in the calculation of the reduced temperature for solar thermal collectors
G	In-plane irradiance (kJ/(h·m^2))
m	Flowrate (kg/h)
Ns	Number of cells in series
P	Power (W)
T	Temperature (°C)
T_a	Ambient temperature (°C)
T_{rise}	Air temperature rise (°C)
T*	Characteristic temperature (°C)
$(T^*-T_a)/G$	Reduced temperature (°C·h·m^2/kJ)
U_L*	Collector heat loss coefficient with characteristic temperature T* in reduced

	temperature for solar thermal collectors (kJ/(h·m^2·°C))
$\overline{U_L}^*$	Collector heat loss coefficient with characteristic temperature T^* in reduced temperature for PV/T collectors (kJ/(hm^2·°C))
V_{oc}	Open-circuit voltage (V)

Greek Symbols

β_{Voc}	Open-circuit voltage temperature coefficient (V/°C)
η	Efficiency
γ_{mpp}	Maximum power point temperature coefficient (W/°C)
$\gamma_{mpp,rel}$	Relative maximum power point temperature coefficient (1/°C)
$(\tau\alpha)_e$	Effective transmittance-absorptance product for solar thermal collectors
$\overline{(\tau\alpha)_e}$	Effective transmittance-absorptance product for PV/T collectors

Subscripts

a	Aperture
fm	Mean fluid
g	Gross
i	Inlet
L	Leakage
o	Outlet
PV	PV
PV,ref	Reference PV
PV,back_AVG	PV back surface average (°C)
th	Thermal
mpp	Maximum power point

Abbreviation

ECT	Equivalent cell temperature
MLR	Multiple linear regression
NOCT	Norminal operating cell temperature
STC	Standard testing conditions

Appendices

Appendix A

The coefficient of correlation, R^2, is expressed as:

$$R^2 = 1 - \frac{\sum_{i=1}^{n} \left(y_{observed,i} - y_{predicted,i}\right)^2}{\sum_{i=1}^{n} \left(y_{observed,i} - \bar{y}\right)^2} \tag{10}$$

In Eq. (10), n is the total number of observations, $y_{observed,i}$ is the i^{th} observed value, $y_{predicted,i}$ is the i^{th} value predicted by the model and $\bar{y}$ is the average of the n observed values. The mean bias error, MBE, and root mean square error, RMSE, are given as:

$$MBE = \frac{1}{n}\sum_{i=1}^{n}\left(y_{observed,i} - y_{predicted,i}\right) \tag{11}$$

$$RMSE = \sqrt{\frac{1}{n}\sum_{i=1}^{n}\left(y_{observed,i} - y_{predicted,i}\right)^2} \tag{12}$$

These errors can also be expressed as a percentage of the mean:

$$MBE\% = \frac{MBE}{\bar{y}} * 100 \tag{13}$$

$$RMSE\% = \frac{RMSE}{\bar{y}} * 100 \tag{14}$$

Appendix B

Uncertainties can be divided into Type A and Type B uncertainties. Type A uncertainties are obtained from statistical methods and Type B are evaluated by using other information such as manufacturer's specifications or calibration certificates. Type A standard uncertainty, u_A, is obtained from the same measurement taken several times. For bias-free measurement, it is given as:

$$u_A = \frac{s}{\sqrt{n}} \tag{15}$$

In Eq. (15), s is the standard deviation expressed as:

$$s = \sqrt{\frac{\sum_{i=1}^{n}\left(y_{observed,i} - \bar{y}\right)^2}{n-1}} \tag{16}$$

The evaluation of a standard uncertainty of Type B, u_B, will vary with the type of estimate. A detailed explanation of the calculation of Type B uncertainties can be found in [22]. The combined standard uncertainty, u_c, combines both Type A and Type B estimates. For a value calculated using a function f, the combined uncertainty u_c can usually be simplified to Eq. (17) if the nonlinearity of f can be neglected.

$$u_c = \sqrt{\sum_{i=1}^{n}\left(\frac{\partial f}{\partial y_i}\right)^2 u^2\left(y_i\right)} \tag{17}$$

In Eq. (17), the standard uncertainty u can be a Type A or a Type B uncertainty. The combined standard uncertainty is equivalent to one standard deviation or to the uncertainty for a confidence level of 68%. In order to express this uncertainty for other confidence levels, it can be multiplied by a coverage factor k. The result of this multiplication gives the expanded uncertainty, U:

$$U = ku_c \tag{18}$$

For a confidence level of 95%, k=2 and for a confidence level of 99%, k=2.58.

This method was used in this study to compute the expanded uncertainty which is what is represented with the bars on the graphs. For all measurements or computed values, a confidence level of 95% was used.

References

[1] International Energy Agency (IEA), 2010, "Energy Technology Perspectives," OECD/IEA, Paris, France.

[2] PV Catapult, 2006, "PVT Roadmap A European Guide for the Development and Market Introduction for PV-Thermal Technology", http:/ /www.pvtforum.org/pvtroadmap.pdf.

[3] Noguchi, M., Athienitis, A., Delisle, V., Ayoub, J., and Berneche, B, 2008, "Net Zero Energy Homes of the Future: A Case Study of the EcoTerra™ Home in Canada," *Renewable Energy Congress*, Glasgow, Scotland.

[4] Pogharian, S., Ayoub, J., Candanedo, J., and Athienitis, A, 2008, "Getting to a Net Zero Energy Lifestyle in Canada: The Alstonvale Net Zero house," *23rd European PV Solar Energy Conference*, Valencia, Spain.

[5] Athienitis, A., Bambara, J., O'Neill, B., and Faille, J., 2010, "A Prototype Photovoltaic/Thermal System Integrated with Transpired Collector," Solar Energy, **85** (1), pp. 139-153.

[6] Zondag, H.A, 2008, "Main R&D Issues for PVT-A manufacturer's perspective," Report DC2 subtask C of IEA SHC Task 35 on PV/Thermal Systems.

[7] International Electrotechnical Commission, 2005, "Crystalline Silicon Terrestrial Photovoltaic (PV) Modules – Design Qualification and Type Approval," IEC 61215-2, International Electrotechnical Commission.

[8] International Electrotechnical Commission (IEC), 1998, "Thin-Film Terrestrial Photovoltaic (PV) Modules – Design Qualification and Type Approval," IEC 61646, International Electrotechnical Commission.

[9] American Society of Heating, Refrigerating and Air-Conditioning (ASHRAE), 2010, "Methods of Testing to Determine the Thermal Performance of Solar Collectors," ANSI/ASHRAE 93-2010.

[10] Hottel, H.C, and Whillier, A., 1958, "Evaluation of Flat-Plate Solar Collector Performance," *Transactions of the Conference on the Use of Solar Energy,* University of Arizona Press, Tucson, Arizona, pp. 74-104.

[11] European Committee for Standardization, 2005, "Thermal Solar Systems and Components – Solar Collectors – Part 2: Test methods," EN 12975-2, European Committee for Standardization.

[12] Buchinger, J., 2006, "Recommendations on Testing of Solar Air Collectors," Technical Report WP 4.1 D2, D3, European Commission – New Generation of Solar Thermal Systems.

[13] Sandnes, B., and Rekstad, J., 2002, "A Photovoltaic/Thermal (PV/T) Collector with a Polymer Absorber Plate Experimental Study and Analytical Model," Solar Energy, **72**, pp. 63-73.
[14] Zondag, H.A., De Vries, D.W., Van Helden, W.G.J., and Van Zolingen, R.J.C., 2002, "The Thermal and Electrical Yield of a PV-Thermal Collector," Solar Energy, **72**, pp. 113-128.
[15] Tonui, J.K., and Tripanagnostopoulos, Y., 2007, "Improved PV/T Solar Collectors with Heat Extraction by Forced or Natural Air Circulation," Renewable Energy, **32**, pp. 623-637.
[16] Othman, M.Y., Yatim, B., Sopian, K., and Abu Bakar, M.N, 2007, "Performance Studies on a Finned Double-Pass Photovoltaic-Thermal (PV/T) Solar Collector," Desalination, **209**, pp. 43-49.
[17] PV Catapult, 2005, "D8-6: PVT Performance Measurements Guidelines," Contract no: 502775 (SES6), http://www.pvtforum.org/D8-6_PV_%20performance_measurement_guidelines.pdf.
[18] International Agency Solar Heating & Cooling Programme Task 35, http://www.iea-shc.org/task35/.
[19] Collins, M., 2008, "Recommended Standard for Characterization and Monitoring of PV/Thermal Systems," Report DB2-IEA subtask B of IEA SHC Task 35 on PV/Thermal Solar Systems.
[20] International Electrotechnical Commission (IEC), 1993, "Determination of the Equivalent Cell Temperature (ECT) of Photovoltaic (PV) Devices by the Open-Circuit Voltage Method," IEC 60904-5, International Electrotechnical Commission.
[21] Florschuetz, L.W, 1979, "Extension of the Hottel-Whillier Model to the Analysis of Combined Photovoltaic/Thermal Flat Plate Collectors," Solar energy, **22**, pp.361-366.
[22] International Organization for Standardization, 1995, *Guide to the Expression of Uncertainty in Measurement*, Switzerland, pp. 1-101.